

Transmission Bows of Radially Inhomogeneous Spheres

JAMES A. LOCK^{1,*} AND PHILIP LAVEN²

¹ (Retired) Physics Dept., Cleveland State University, Cleveland, OH 44115, USA

² Russells Crescent, Horley, RH6 7DJ, United Kingdom

*Corresponding author: j.lock@csuohio.edu

Received 17 January 2017; revised 2 April 2017; accepted 2 April 2017; posted 4 April 2017 (Doc. ID 284905); published 25 April 2017

We consider transmission scattering of a plane wave by a radially inhomogeneous sphere containing a localized region of refractive index decrease. In ray theory, the boundary conditions on the deflection angle at axial and grazing incidence determine that transmission scattering gives rise to an even number of bows, half of them being relative maximum bows and half being relative minimum bows. For a model refractive index profile, we determine the conditions under which different numbers of bows occur, and we suggest physical mechanisms responsible for producing them. We also verify that these bows occur in wave scattering in the short wavelength limit, both in the frequency-domain and in the time-domain. © 2017 Optical Society of America

OCIS codes: 080.5692 (ray trajectories in inhomogeneous media), 260.2710 (inhomogeneous optical media), 290.4020 (Mie theory), 290.5825 (scattering theory).

<http://dx.doi.org/10.1364/AO.99.099999>

1. INTRODUCTION

For scattering of a monochromatic electromagnetic plane wave by a homogeneous dielectric spherical particle in the short wavelength limit, the ray theory deflection angle for transmission is a monotonically increasing function of the angle of incidence. A bow (commonly called a rainbow if the spherical particle is a small falling water drop in a rain shower that is illuminated by sunlight) occurs in ray theory when the deflection angle possesses a relative minimum, which is the usually encountered case, or a relative maximum. Thus no bows occur for transmission scattering for the highly symmetric geometry of a plane wave illuminating a homogeneous sphere [1, 2]. Since a plane wave can be thought of as originating from a point source an infinite distance from the sphere, this statement must be revised for scattering of the radially outgoing rays emanating from a point source located a finite distance from the homogeneous sphere. The transmission bow in this case results from the opening up to the far-zone of the formerly near-zone spherical aberration caustic [3]. The statement must also be revised for scattering of a plane wave having end-on incidence when the sphere is deformed into a prolate spheroid. The pair of transmission bows in this case result from the spherical aberration caustic turning itself inside-out [3, 4]. In each of these cases, the transmission bows result from symmetry breaking for either the incident beam or the spherical particle.

The statement must also be revised for yet another case of symmetry breaking, i.e. when a plane wave is incident on a radially inhomogeneous sphere. In this case either a transmission bow, or a pair of transmission bows, have been predicted for certain refractive index profiles [5-8]. The purpose of this study is to examine transmission scattering of a plane wave by a radially inhomogeneous

sphere from a more general point of view. We determine a set of boundary conditions for the deflection angle that allow two or more transmission bows to occur, and we suggest physical mechanisms responsible for producing the bows.

The body of this study proceeds as follows. In Sec. 2 we obtain a set of boundary conditions for the transmission deflection angle as a function of the ray angle of incidence for both axial and grazing ray incidence. These boundary conditions dictate that only certain numbers of bows can occur. In Sec. 3 we consider a refractive index profile that decreases in a single localized radial interval. We find that for different values of the steepness of the decrease, either zero bows or two bows will occur, i.e., a relative maximum bow followed by a relative minimum bow. In Sec. 4 we relate the relative maximum bow to the near-onset of the phenomenon of orbiting [9-13], and the relative minimum bow to increased refraction of rays whose trajectory passes through only the outer portion of the refractive index transition region. In Sec. 5 we validate the ray theory results by computing Lorenz-Mie scattering by a finely-stratified sphere having the refractive index profile considered in Sec. 3. In order to gain further information about the bows in the context of wave scattering, we compute time-domain scattering of a short incident pulse by the radially inhomogeneous sphere. From these results we suggest the overall caustic morphology of the two transmission bows. In Sec. 6 we consider a refractive index profile containing two localized radial intervals of refractive index decrease. This results in four transmission bows, a pair of relative maximum bows and a pair of relative minimum bows. In Sec. 7 we recount the principal results of this study. Finally, in Appendix A we derive the ray theory signature of a bow in the time-domain.

2. GENERAL CONSIDERATIONS

We consider scattering of an electromagnetic plane wave of field strength E_0 traveling in vacuum in the $+z$ direction and polarized in the x direction which is incident on a radially inhomogeneous sphere of radius a and refractive index profile $m(r)$ centered on the origin of coordinates. We consider the sphere to be a material particle with $m(r) > 1$ rather than a bubble with $0 < m(r) < 1$. The plane wave may be considered as a collection of parallel light rays crossing the $z = 0$ plane different distances r from the origin with $0 \leq r < \infty$. The positive angle of incidence of a light ray at the sphere surface θ_i , and the positive sense of the deflection angle θ are shown in Fig. 1. In this study we consider only transmission scattering where a ray with the angle of incidence θ_i is refracted into the sphere, travels a curved trajectory inside the radially inhomogeneous particle, and is transmitted out in the θ direction having not undergone any internal reflections. The method of analysis described here can be extended to various numbers of internal reflections.

Application of the formula of Bouguer gives the ray deflection angle for transmission as [14, 15]

$$\theta(\theta_i) = -\pi + 2\theta_i + 2 \sin(\theta_i) \int_{w_T}^1 (dw/w) [\eta^2(w) - \sin^2(\theta_i)]^{-1/2}. \quad (1)$$

We define

$$w \equiv r/a \quad (2)$$

so as to have dimensionless quantities. In addition, the behavior of the function

$$\eta(w) \equiv w m(w) \quad (3)$$

will be found to be of great significance. The closest approach of the interior ray to the center of the sphere, i.e. the classical turning point, is w_T with

$$\eta(w_T) = \sin(\theta_i). \quad (4)$$

In classical mechanics, Eq. (1) also describes the trajectory of a point mass having energy E , and acted on by a conservative central force whose potential energy function is $U(r)$, with the correspondence $m^2(r) \leftrightarrow 1 - U(r)/E$.

$$(5)$$

By differentiating Eq. (5), a decreasing refractive index, $dm/dw < 0$, corresponds to an attractive force, and an increasing refractive index, $dm/dw > 0$, corresponds to a repulsive force. In this study we consider only $dm/dw \leq 0$.

The transmission deflection angle of Eq. (1) exhibits five basic properties. First,

$$\theta(0^\circ) = 0. \quad (6)$$

This says that the axial ray with $\theta_i = 0^\circ$ enters the sphere without refraction, travels in a straight line inside, and exits without refraction. This result is intuitively sensible. It can also be derived from Eq.(1) by (i) assuming that θ_i is small, (ii) substituting this condition into the denominator and the lower limit of integration of the third term, (iii) evaluating the resulting integral exactly, and then (iv) taking the limit $\theta_i \rightarrow 0$. This contribution cancels the first term on the right hand side of Eq.(1), giving Eq.(6).

Second, the initial slope of $\theta(\theta_i)$ is positive,

$$(d\theta/d\theta_i)_{\theta_i=0} > 0. \quad (7)$$

This is most easily demonstrated by appealing to the correspondence with a point mass in the field of an attractive force of Eq. (5). The trajectory of the point mass always curves toward the force center rather than away from it in such a way as to conserve energy and angular momentum. Thus, for an attractive force the point mass always goes around the force center, rather than cutting across in front of it. In the optical case, a ray path always curves toward the region of higher refractive index.

Third, as long as $\eta(w)$ is a monotonically increasing function for $0 \leq \eta \leq 1$,

$$\theta(\theta_i) < \infty \text{ for all } \theta_i. \quad (8)$$

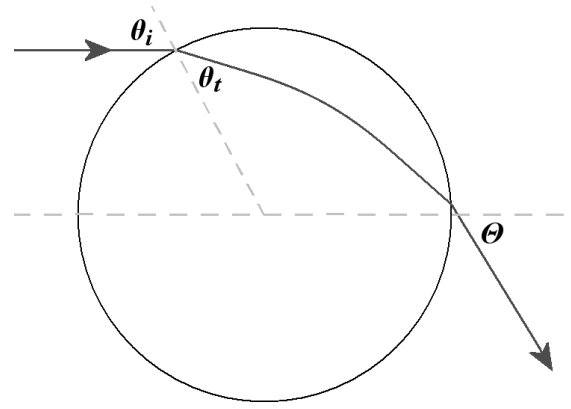


Fig. 1 Geometry of a ray transmitted through a sphere of radius a . The impact parameter of the ray is $\sin(\theta_i)$, and the deflection angle is θ .

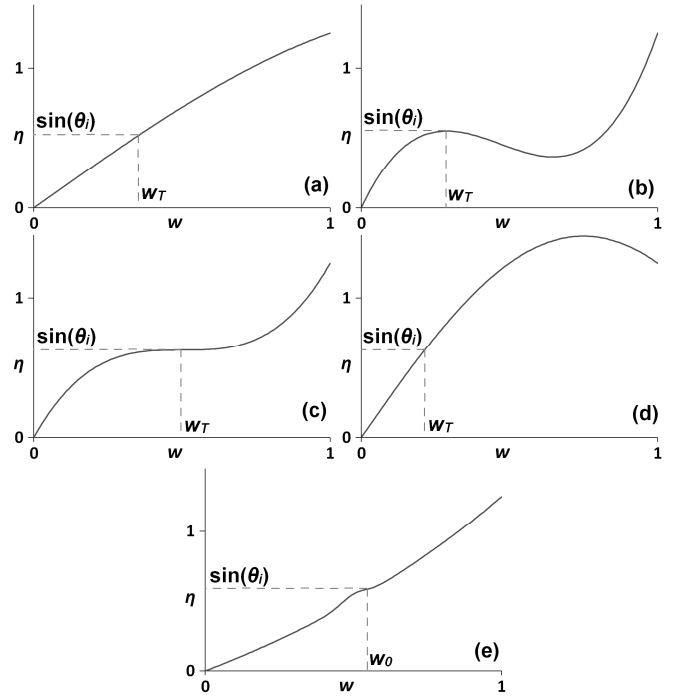


Fig.2 Various behaviors of the function $\eta(w)$ of Eq.(3).

This condition rules out the possibility of the phenomenon of orbiting [9-13]. Since $\eta(w_T) = \sin(\theta_i)$, a potential divergence occurs at the lower limit of integration in Eq. (1). As long as $\eta(w)$ is locally linear in the vicinity of w_T , as is the case in Fig. 2(a), the integrand will be proportional to $(w - w_T)^{-1/2}$ there. When integrated, the contribution of the lower limit of integration is zero, and the entire value of the integral is due to from the upper limit, with θ remaining finite. But if $\eta(w)$ is locally quadratic or cubic in the vicinity of w_T , as is the case in Figs. 2(b, c) respectively, the integrand is proportional to $(w - w_T)^{-1}$ or $(w - w_T)^{-3/2}$ there. When integrated, the lower limit diverges either logarithmically or to the $-1/2$ power, giving $\theta \rightarrow \infty$. This is interpreted as the trajectory of the light ray orbiting around inside the sphere forever, and will be discussed in more detail in Sec. 4a. As a side note, orbiting is also familiar in quantum mechanical atom-atom scattering [16, 17] and scattering of an alpha particle by a nucleus [17], and in scattering of an electromagnetic plane wave by a Luneburg lens [18].

Since $0 \leq \sin(\theta_i) \leq 1$, Eq. (4) dictates that the function $\eta(w)$ must be locally linear in the vicinity of w_T for $0 \leq \eta(w) \leq 1$, i.e. $\eta(w)$ must be

monotonically increasing over this interval. Expressed in a more physical way, although we are assuming that $m(w)$ decreases as a function of w , it cannot decrease too fast, or else the decrease in $m(w)$ will overpower the increase in w in Eq. (3). Lastly, since $m(w) > 1$, one has $\eta(1) > 1$. The η function need not be monotonically increasing for $1 < \eta(w) \leq \eta(1)$, as is illustrated in Fig. 2(d), since this region does not correspond to an angle of incidence via Eq. (4).

Fourth, for grazing incidence one has

$$\theta(\pi/2) > 0. \quad (9)$$

This can be seen by substituting $\theta_i = \pi/2$ into Eq. (1) and using the fact that the integral has already been found to be finite.

Fifth, the final slope of $\theta(\theta_i)$ is

$$(d\theta/d\theta_i)_{\theta_i=\pi/2} = 2. \quad (10)$$

Equation (1) has θ_i dependence in four places, including the θ_i dependence of w_T in the lower limit of integration via Eq. (4). When the derivative of Eq. (1) is evaluated at $\theta_i = \pi/2$, the divergence in two of the terms cancels, resulting in Eq. (10).

Now that we have determined the way in which the graph of $\theta(\theta_i)$ begins at $\theta_i = 0$ and ends at $\theta_i = \pi/2$, the behavior of θ between these two end points depends on the details of the refractive index profile $m(w)$. The deflection angle can be monotonically increasing, which is the case for a constant refractive index. Other possibilities allow for a relative maximum followed by a relative minimum, or a pair of alternating relative maxima and relative minima, etc. Only an even number of transmission bows can occur for a radially inhomogeneous particle having a decreasing refractive index and $\eta(w)$ being monotonically increasing for $0 \leq \eta \leq 1$. The condition of Eq. (8) prohibits an orbiting divergence in $\theta(\theta_i)$. Examples of all of these behaviors are encountered in Secs. 3, 6.

An example of the situation described by Eqs. (6-10) is the two bows in region η of parameter space for the generalized Luneburg sphere described in [8, 19]. The method of analysis described here for determining the number of possible transmission bows can be extended to other classes of refractive index profiles, including an edgeless radially inhomogeneous particle of decreasing refractive index for which $m(1) = 1$, with $\eta(w)$ monotonically increasing for $0 \leq \eta \leq 1$, and $0 < (d\eta/dw)_{w=1} < 1$. This system has an odd number of bows. An example is the single bow for the generalized Luneburg sphere in region γ of parameter space as described in [8, 19, 20]. Another class is a radially inhomogeneous bubble (i.e. $0 < m(w) < 1$) having an increasing refractive index and with $\eta(w)$ monotonically increasing for $0 \leq \eta \leq \eta(1)$. The angle of incidence for critical external reflection is given by $\sin(\theta_c) = \eta(1)$. This system has an even number of bows. An example is the two bows for the generalized Luneburg sphere in region ξ of parameter space as described in [8, 19]. Yet another class is an edgeless radially inhomogeneous bubble with an increasing refractive index for which $m(1) = 1$. If $\eta(w)$ is also monotonically increasing for $0 \leq \eta \leq 1$ and $(d\eta/dw)_{w=1} > 1$, the system has an odd number of bows. An example is the single bow for the generalized Luneburg sphere in region δ of parameter space as described in [8, 19]. Refractive index classes where an incident ray refracts one way at the sphere surface and the other way once inside require more care when applying the method of analysis used here. Examples of these classes are regions ν and ψ for a generalized Luneburg sphere as described in [19].

3. MODEL REFRACTIVE INDEX PROFILE

In order to explore the possibilities of the number of transmission bows described in Sec. 2, we consider the following refractive index profile having the four adjustable parameters D, R, M , and H ,

$$\begin{aligned} m(w) &= M + H && \text{for } 0 \leq w \leq D - R \\ &= M - H \sin[(W - D)\pi / (2R)] && \text{for } D - R \leq w \leq D + R \\ &= M - H && \text{for } D + R \leq w \leq 1. \end{aligned} \quad (11)$$

This radially inhomogeneous sphere is divided into three concentric regions. The innermost region has a large, constant refractive index. The middle, or transition, region has a smooth decrease to the small, constant refractive index of the outermost region. This profile is shown in Fig. 3. The profile varies smoothly, with both $m(w)$ and dm/dw being continuous everywhere. The greatest slope occurs at $w = D$, and the steepness of the transition can be parameterized by H/R .

Substituting Eq. (11) into Eq. (1) and performing the integral numerically, representative results for the ray theory deflection angle as a function of the angle of incidence are given in Fig. 4(a) for $D = 0.333$, $M = 1.558$, $H = 0.142$ and $0.05 \leq R \leq 0.30$. The near-onset of orbiting is evident for $R = 0.05$, with relative maximum and relative minimum bows occurring at $\theta \approx 177^\circ$ and $\theta \approx 20^\circ$. In order to provide a more detailed view of the coalescence and extinguishing of the two bows when $R \approx 0.30$, Fig. 4(b) shows the deflection angle for the same values of D, M, H and $0.28 \leq R \leq 0.34$. In Fig. 4(b) it is seen that the final occurrence of an inflection point of $\theta(\theta_i)$ is for $R = 0.32$, signaling the coalescence of the two bows. For $R = 0.05, 0.12, 0.20, 0.25, 0.30$, and 0.32 the deflection angles of the relative maximum and relative minimum bows are given in Table 1. Both a relative maximum transmission bow and a relative minimum bow occur when the refractive index decrease is relatively steep, $0.44 < H/R < 2.93$, and no transmission bows occur when the refractive index decrease is relatively gentle, $0 \leq H/R < 0.44$. There is nothing special about the particular values of D, R, M , and H chosen here. The specific reason for their choice will become apparent in Sec. 6. A nearly identical evolution from two transmission bows to zero bows was found to occur for a wide range of parameters used with Eq. (11).

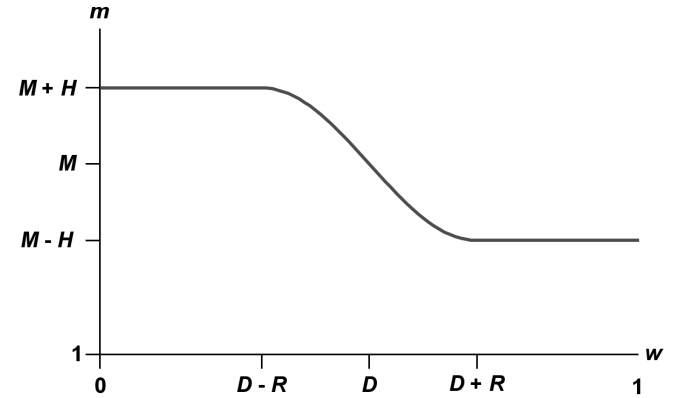


Fig. 3. Model refractive index profile of Eq. (11).

Table 1: The value of the independent parameter R for $D = 0.333$, $M = 1.558$, and $H = 0.142$, the deflection angles of the relative maximum and minimum bows from Fig. 4.

R	$\theta_{\text{maximum bow}}$	$\theta_{\text{minimum bow}}$
0.05	177°	20°
0.12	61°	26°
0.20	47°	33°
0.25	43°	38°
0.30	42.3°	41.4°
0.32	42.3°	42.3°

4. INTERPRETATION OF THE TRANSMISSION BOWS

4a. Relative maximum bow

In this subsection we show that the maximum bow results from a steep, localized decrease in the refractive index so that $\eta(w)$ has a correspondingly slow, localized increase, producing the near-onset of orbiting. In Ref. [21] this near-onset was termed a deep rainbow. This interpretation can be motivated by the following general argument. We consider the value of the integral of Eq. (1) over an interval in w adjacent to a ray's classical turning point w_T . We assume that for $w_T \leq w \leq w_T + \Delta$ the function $\eta(w)$ can be well approximated by the first two terms of its Taylor series expansion

$$\eta(w) \approx \eta(w_T) + s(w - w_T), \quad (12)$$

where s is the slope of $\eta(w)$ at w_T . The contribution of this interval to the integral in Eq. (1) is proportional to $(\Delta^{1/2}/w_T) [d(\eta^2)/dw]^{-1/2}_{w_T}$. Let $s_0 > 0$ be the minimum slope of the $\eta(w)$ function, which occurs at $w = w_0$ with $0 < \eta(w_0) < 1$ as in Fig. 2(e). In like manner, the contribution of this interval to the integral is proportional to $(\Delta^{1/2}/w_0) [d(\eta^2)/dw]^{-1/2}_{w_0}$. It should be noted that if $s_0 = 0$ and $\eta(w)$ is locally cubic about w_0 as in Fig. 2(c), i.e.

$$\eta(w) \approx \eta(w_0) + t(w - w_0)^3 \quad (13)$$

the contribution of the interval $w_0 \leq w \leq w_0 + \Delta$ to the integral diverges, and corresponds to orbiting. If s_0 is sufficiently small so that

$$[d(\eta^2)/dw]_{w_0} \ll [d(\eta^2)/dw]_{w_T}, \quad (14)$$

the contribution to the integral near the lower limit of integration has a sharp maximum. This suggests that the relative maximum bow is a pre-orbiting condition connected with the minimum of the slope of $\eta^2(w)$.

The results for the refractive index profile of Eq. (11) confirm this interpretation. For the values of D , W , and H of Fig. 4(a), the minimum slope of $\eta(w)$ was numerically found to vanish when $R = 0.0485$ or $H/R = 2.93$, giving the orbiting condition. The orbiting condition can also be estimated analytically. Taylor series expanding $\eta(w)$ of Eq. (11) in powers of

$$\varepsilon \equiv w - D \quad (15)$$

we obtain

$$\eta(\varepsilon) = DM + [M - \pi DH/(2R)] \varepsilon - [\pi H/(2R)] \varepsilon^2 + [\pi^3 DH/(48R^3)] \varepsilon^3 + O(\varepsilon^4). \quad (16)$$

$$\text{Orbiting should occur when } d\eta/d\varepsilon = 0 \text{ and } d^2\eta/d\varepsilon^2 = 0, \text{ or when } H/R \approx (2M/\pi D) [1 - 2H^2/M^2 + O(H^4/M^4)]. \quad (17)$$

For the values of D , M , and H considered above, one obtains $H/R = 2.929$ in agreement with result obtained numerically. Thus the value $R = 0.05$ or $H/R = 2.84$ which produced the large relative maximum in Fig. 4(a), is close to the orbiting condition.

As was mentioned above, the greatest slope of the refractive index profile occurs at $w = D = 0.333$. For the values of D , W , and H of Fig. 4(a) and $R = 0.05, 0.12, 0.20, 0.25$, and 0.30 , the location w_0 of the minimum slope of $\eta(\varepsilon)$ was numerically determined, and is given in Table 2. It starts out being quite close to D , and then increasingly deviates from it. The numerically determined value of $\eta(w_0)$ is also given in Table 2. If the relative maximum bow occurred at the minimum of $d\eta/dw$, the angle of incidence of the rainbow ray would be $\sin(\theta_i) = \eta(w_0)$. In order to test this prediction, the impact parameter of the relative maximum bow from Fig. 4(a) is also given in Table 2. The correspondence is close when the deflection angle has a high, narrow peak, and progressively weakens as the deflection angle peak broadens.

4b. Relative minimum bow

In order to satisfy the boundary conditions on $\theta(\theta_i)$ at $\theta_i = 0^\circ$ and $\theta_i = 90^\circ$, the existence of a relative maximum bow demands the existence of an associated relative minimum bow. In this subsection we show that

the relative minimum bow is associated with the tapering off of the refractive index decrease at the outer edge of the transition region of Fig. 3. This interpretation is motivated as follows. For a particle of constant refractive index $M - H$, the transmission deflection angle is

$$\theta = 2(\theta_i - \theta_t) \quad (18)$$

where

$$\sin(\theta_t) = (M - H) \sin(\theta_i) \quad (19)$$

by Snell's law. This deflection angle is a monotonically increasing function of the angle of incidence θ_i . However, for the time being it is more convenient to consider it as a monotonically decreasing function of θ_i as it decreases from 90° toward 0° . For the refractive index profile of Eq. (11), incoming rays having a large impact parameter traverse only the outer region of the sphere until refraction at the outer surface causes the interior ray to graze the outer edge of the transition region. This occurs when

$$\sin(\theta_i) = (M - H)(D + R). \quad (20)$$

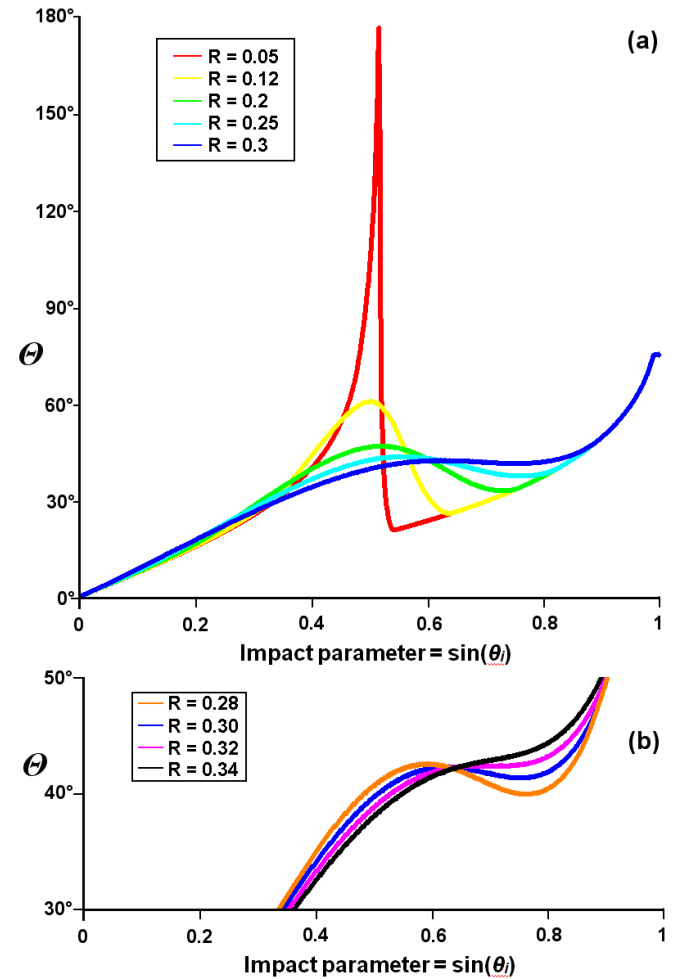


Fig. 4. (Color online) Ray theory deflection angle θ as a function of $\sin(\theta)$ for the refractive index profile of Eq. (11) with $D = 0.333$, $M = 1.558$, $H = 0.142$, and (a) $0.05 \leq R \leq 0.30$, and (b) $0.28 \leq R \leq 0.34$.

Table 2: The value of the independent parameter R for $D = 0.333$, $M = 1.558$, and $H = 0.142$, the value of w_0 and $\eta(w_0)$ for the minimum of $d\eta/dw$ numerically obtained from Eq. (11), the impact parameters $\sin(\theta_i)$ of the relative maximum and minimum bows from Fig. 4, and the impact parameter for grazing incidence at the end of the region of refractive index decrease from Eq. (20). The third and fourth, and the fifth and sixth columns are to be compared to each other.

R	w_0	$\eta(w_0)$	$\sin(\theta_i)$	$\sin(\theta_i)$	$\sin(\theta_i)$
	max bow	max bow	max bow	min bow	Eq. (20)
0.05	0.341	0.519	0.52	0.54	0.542
0.12	0.363	0.546	0.51	0.64	0.641
0.20	0.403	0.598	0.53	0.73	0.755
0.25	0.433	0.638	0.57	0.77	0.826
0.30	0.468	0.686	0.65	0.75	0.896

For rays with a slightly smaller angle of incidence than in Eq. (20), the ray trajectory increasingly penetrates into the transition region where the refractive index progressively increases. This leads to increased refraction in the transition region and thus a tendency for its contribution to θ to increase. This tendency eventually overtakes the continued decrease in θ , had the refractive index continued to be $M - H$, producing the relative minimum bow. We consider an analytical example that illustrates this point. In the transition region of Fig. 3 we chose to model the $\eta(w)$ function as

$$\eta(w) = (M - H)w + \alpha(w - D - R)^2. \quad (21)$$

The first term extrapolates the constant refractive index of the outer region to the transition region, and the second term is a quadratic rise in $\eta(w)$ over this baseline. We let

$$w_T = D + R - \Delta. \quad (22)$$

Substitution of Eqs.(21, 22) into Eq. (1), Taylor series expanding the integrand, and integrating term by term gives

$$\theta(\theta_i) = 2(\theta_i - \theta_i) + 2^{1/2} (8/3) \{ \alpha / [(M - H) (D + R)^{1/2}] \} \Delta^{3/2} + O(\Delta^{5/2}). \quad (23)$$

As θ_i decreases and Δ increases, the first term in Eq. (23) decreases while the second term increases at a faster rate, eventually overtaking the decrease of the first term. Similarly, if we were to model $\eta(w)$ in the transition region by

$$\eta(w) = (M - H)w - \beta(w - D - R)^3, \quad (24)$$

substitution of Eqs.(22, 24) into Eq. (1), Taylor series expanding the integrand, and integrating term by term gives

$$\theta(\theta_i) = 2(\theta_i - \theta_i) + 2^{1/2} (16/5) \{ \beta / [(M - H) (D + R)^{1/2}] \} \Delta^{5/2} + O(\Delta^{7/2}). \quad (25)$$

Again as θ_i decreases and Δ increases, the first term in Eq. (25) decreases while the second term increases at a faster rate, eventually producing a relative minimum of the deflection angle. The $(p-1)$ -order bows of a *homogeneous* sphere can also be interpreted in terms of a competition between the portion of the ray deflection due to refraction and the portion due to internal reflection. Similarly, the condition for orbiting in classical mechanics can be interpreted in terms of a competition between the attractive central force and the repulsive centrifugal force.

As a numerical test of the prediction of the previous paragraph, the relative minimum bow for $R = 0.05, 0.12, 0.20, 0.25$, and 0.30 occurs in Fig. 4(a) at the value of $\sin(\theta_i)$ given in Table 2. The competition producing this bow discussed above suggests that it occurs at an angle of incidence slightly below the value given by Eq. (20), which is also given in Table 2. The agreement between the results of Fig. 4(a) and the prediction of Eq. (20) is quite good, especially for values of R relatively close to the onset of orbiting.

5. TRANSMISSION BOWS IN WAVE THEORY

5a. Scattered intensity and time-domain scattering

The transmission deflection angle as a function of angle of incidence in ray theory for another set of parameters of Eq. (11), $D = 0.5$, $R = 0.2$, $M = 1.5$, and $H = 0.25$ is shown in Fig. 5. A well-formed relative maximum bow occurs at $\sin(\theta_i) \approx 0.75$ and $\theta \approx 121^\circ$, and a well-formed relative minimum bow occurs at $\sin(\theta_i) \approx 0.87$ and $\theta \approx 33^\circ$. In order to test the mechanisms suggested in Sec. 4 for the relative maximum and relative minimum bows, the minimum slope of $\eta(w)$ was numerically found to occur at $w_0 = 0.55$ and $\eta(w_0) = 0.772$, in good agreement with the incident impact parameter of the relative maximum bow in Fig. 5. Equation (20) now gives $\sin(\theta_i) = 0.875$, also in agreement with the impact parameter of the relative minimum bow in Fig. 5.

It is of importance to verify that both transmission bows also occur in wave scattering, rather than being merely artifacts of ray theory. To do this, we computed Lorenz-Mie scattering by a finely-stratified sphere having 256 concentric layers whose refractive indices are the discretized version of Eq. (11) with the values of D, R, M, H as above. The transverse electric (TE) polarized scattered intensity was computed for $\lambda = 0.65 \mu\text{m}$ and $a = 100 \mu\text{m}$ using the parallel iteration method described in [22, 23]. The resulting scattered intensity shown in Fig. 6 and includes all the Debye series processes, not just $p = 1$ transmission. Bows at $\theta \approx 34^\circ$ and $\theta \approx 120^\circ$ are clearly visible, with a large number of supernumeraries between them. These are the ray theory transmission bows of Fig. 5. However, the intensity graph cannot distinguish which of these are relative maximum bows and which are relative minimum bows.

The two transmission bows were also studied using time-domain scattering in which a Gaussian pulse of full-width 5 fs and centered on $\lambda = 0.65 \mu\text{m}$ is incident on the layered sphere. The time delay of the scattered signal was computed as a function of deflection angle [24, 25]. Time-domain scattering essentially performs a Debye series decomposition of the scattered intensity of Fig. 6 since scattered light undergoing a larger number of internal reflections is increasingly delayed with respect to shorter path length processes such as $p = 1$ transmission. The time-domain graph for delay times characteristic of transmission are shown in Fig. 7.

Time-domain scattering easily distinguishes whether the bows are relative maximum or relative minimum bows. The ray theory signature of these bows is discussed in Appendix A. The bow with $\theta \approx 34^\circ$ and a delay time of $t \approx 950$ fs is a relative minimum of both the deflection angle and the delay time, while the bow with $\theta \approx 120^\circ$ and $t \approx 1340$ fs is a relative maximum of both. The results of Figs. 6 and 7 clearly verify that the pair of transmission bows initially predicted using ray theory occur as well in wave theory in the short wavelength limit $2\pi a/\lambda \gg 1$.

5b. Coalescence of the two bows and overall caustic morphology

As mentioned above, in Fig. 4(b) the relative maximum and relative minimum bows coalesce and then are extinguished when $R \approx 0.32$. The deflection angle varies over a relatively small range $42.2^\circ \leq \theta \leq 42.5^\circ$ for a relatively wide interval of angles of incidence, $38^\circ \leq \theta_i \leq 49^\circ$, which should lead to exceptionally strong scattering in this small deflection angle interval. In order to verify this ray theory prediction, Fig. 8 shows the TE scattered intensity for $\lambda = 0.65 \mu\text{m}$, $a = 200 \mu\text{m}$, and the refractive index profile of Eq. (11) with the parameters of Fig. 4(b) with $R = 0.32$. Again, the Figure contains the contributions of all the Debye series terms. But the strong, localized scattering peak at $\theta \approx 42.4^\circ$, which rises an order of magnitude above the background

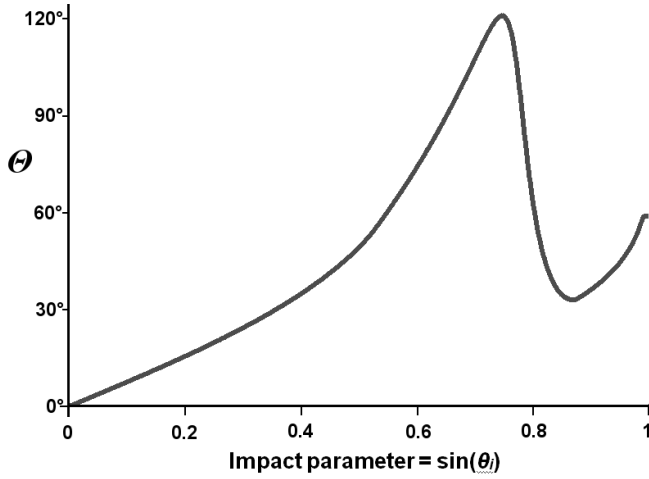


Fig. 5. Ray theory deflection angle θ as a function of $\sin(\theta_i)$ for the refractive index profile of Eq. (11) with $D = 0.5$, $R = 0.2$, $M = 1.5$, and $H = 0.25$.

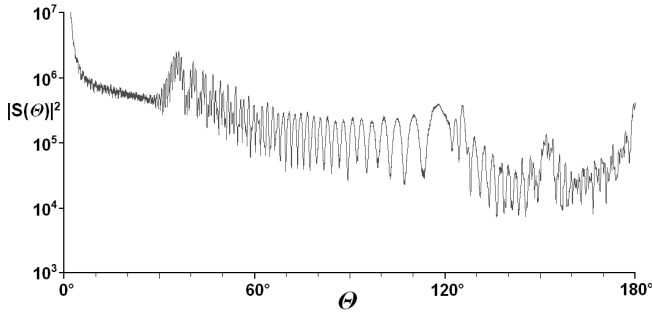


Fig. 6. Wave theory TE scattered intensity as a function of θ for an incident wavelength $\lambda = 0.65 \mu\text{m}$, a sphere of radius $a = 100 \mu\text{m}$, and the refractive index profile of Eq. (11) with $D = 0.5$, $R = 0.2$, $M = 1.5$, and $H = 0.25$. The intensity has been “sun-smoothed” by convolving it with a 0.5° diameter source to remove the high-frequency interference structure.

scattered light, is the signature of the two coalesced transmission bows. It should also be noticed that this peak is not accompanied by supernumeraries. This results from the fact that in Fig. 6 the supernumeraries were located between the two bows. So as the bows coalesce, the supernumeraries between them vanish.

The five simplest structurally stable optical caustics, the fold, cusp, swallowtail, elliptic umbilic, and hyperbolic umbilic have been described and illustrated in many places, e.g. [26-30]. In addition, the butterfly and parabolic umbilic caustics are described and illustrated in [27,28]. The results given in this paper thus far lead to the conjecture that the overarching caustic morphology of the two transmission bows is that of the cusp caustic rather than the fold caustic. This was described in Fig. 12 of [19] in the context of scattering by a generalized Luneburg lens. This Figure is adapted to the present situation as Fig. 9. The fold caustic is a function of one control variable, standardly taken to be the deflection angle θ when applied to scattering by a homogeneous sphere. There is a supernumerary interference pattern to one side of the caustic (i.e. the two-ray region) and no scattered light on the other side (i.e. the zero-ray region).

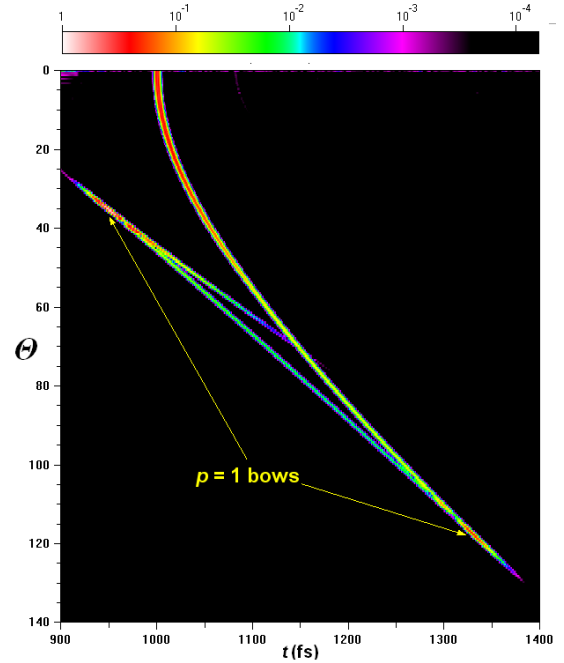


Fig. 7. (Color online) Time-domain TE scattering as a function of θ and the delay time t for a sphere of radius $a = 100 \mu\text{m}$, an incident Gaussian pulse of 5 fs full-width centered on $\lambda = 0.65 \mu\text{m}$, and the refractive index profile used in Fig. 6.

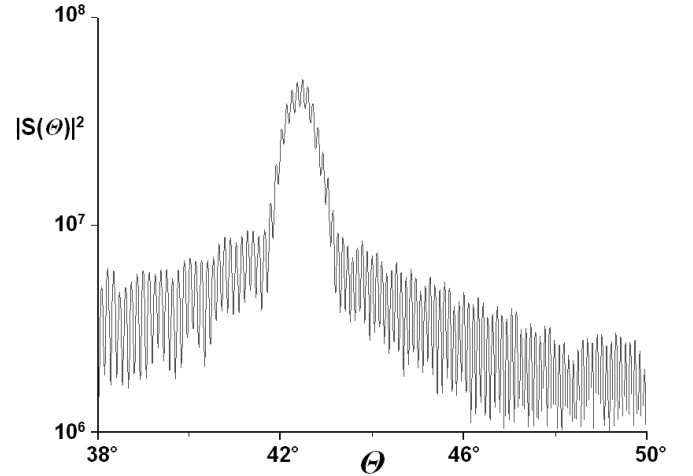


Fig. 8. Wave theory TE scattered intensity as a function of θ for an incident wavelength $\lambda = 0.65 \mu\text{m}$, a sphere of radius $a = 200 \mu\text{m}$, and the refractive index profile of Eq. (11) with $D = 0.3333$, $R = 0.32$, $M = 1.558$, and $H = 0.142$. The large, isolated scattering enhancement centered on $\theta \approx 42.4^\circ$, without the appearance of a surrounding supernumerary interference pattern, is the signature of the coalescence of the two transmission bows of Fig. 6.

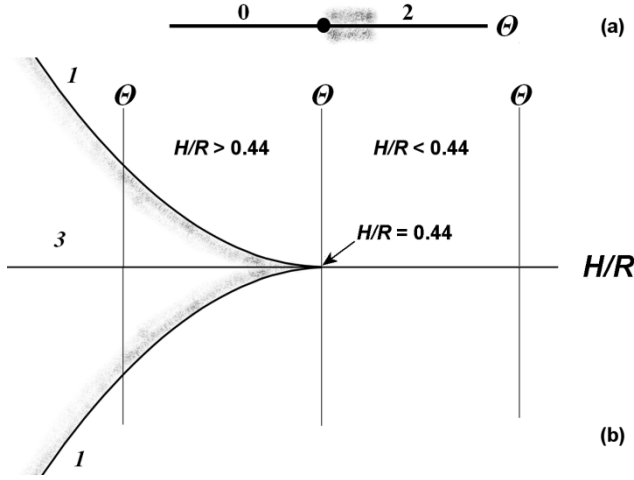


Fig. 9. (a) Fold caustic (large dot) and the scattering angle θ axis. The number of participating rays for each scattering angle is listed, and the shaded region indicates the supernumerary interference pattern. (b) Cusp caustic and the θ and H/R axes. The number of participating rays for each scattering angle is listed, and the shaded region indicates the supernumerary interference pattern. When $H/R > 0.44$ for the refractive index profile of Eq. (11) with $D = 0.333$, $M = 1.558$, and $H = 0.142$, two bows occur at different values of θ . When $H/R = 0.44$, the two bows coalesce at a single value of θ . When $H/R < 0.44$, no bows occur.

The cusp caustic is a function of two control variables, which we here take to be the deflection angle θ and the steepness parameter, H/R , of the localized decrease in the refractive index profile. The cusp caustic consists of two curved fold caustics joined together at a cusp point. The supernumerary interference pattern of the cusp (i.e. the three-ray region) lies inside the cusp, and there is no interference pattern outside the cusp (i.e. the one-ray region). When $H/R > 0.44$ for the values of D , M , and H considered in Fig. 4, the θ axis cuts the cusp caustic twice, exhibiting two bows with the supernumerary interference pattern between them. When $H/R = 0.44$, the θ axis cuts the cusp caustic at the cusp point, exhibiting a large scattered intensity that is not accompanied by supernumeraries. Lastly, when $H/R < 0.44$, the θ axis no longer cuts the cusp caustic, and exhibits no transmission bows. An identical two-bow coalescence phenomenon was described in [31] for $p = 2$ scattering by a tilted homogeneous cylinder, where the second control variable in that case was the cylinder's tilt angle with respect to the direction of the incident plane wave.

6. FOUR TRANSMISSION BOWS

Since a sufficiently steep, localized refractive index decrease leads to a pair of transmission bows, two localized refractive index decreases should be able to lead to two pairs of transmission bows. This was tested using the following refractive index profile

$$\begin{aligned}
 m(w) &= M + 2H_1 & \text{for } 0 \leq w \leq D_1 - R_1 \\
 M + H_1 + H_1 \cos[(w - D_1 + R_1)\pi / (2R_1)] & & \text{for } D_1 - R_1 \leq w \leq D_1 + R_1 \\
 M & & \text{for } D_1 + R_1 \leq w \leq D_2 - R_2 \\
 M - H_2 + H_2 \cos[(w - D_2 + R_2)\pi / (2R_2)] & & \text{for } D_2 - R_2 \leq w \leq D_2 + R_2 \\
 M - 2H_2 & & \text{for } D_2 + R_2 \leq w \leq 1.
 \end{aligned} \quad (26)$$

We used the parameters $D_1 = 0.333$, $R_1 = 0.083$, $D_2 = 0.667$, $R_2 = 0.167$, $M = 1.416$, $H_1 = H_2 = 0.142$ to generate the refractive index profile shown in Fig. 10. The first refractive index decrease of Eq. (26) is identical to that used in Eq. (11) and Fig. 4 but with $R = 0.083$, and which produced a pair of transmission bows. There is now a second refractive index decrease following the first decrease, with half the

value of H/R . Substituting this profile into Eq. (1), the graph of the resulting deflection angle as a function of the angle of incidence is shown in Fig. 11. Two pairs of transmission bows are produced for these parameters. The first relative maximum bow A occurs at $\theta \approx 87^\circ$ and $\sin(\theta_i) \approx 0.51$. The first relative minimum bow B occurs at $\theta \approx 34^\circ$ and $\sin(\theta_i) \approx 0.58$. The second relative maximum bow C occurs at $\theta \approx 105^\circ$ and $\sin(\theta_i) \approx 0.84$. Finally, the second relative minimum bow D occurs at $\theta \approx 28^\circ$ and $\sin(\theta_i) \approx 0.94$. If only the first refractive index step had been present, the relative maximum bow A would have occurred at $\theta \approx 79^\circ$ and $\sin(\theta_i) \approx 0.51$, and the relative minimum bow B would have occurred at $\theta \approx 23^\circ$ and $\sin(\theta_i) \approx 0.59$. In like manner, if only the second refractive index step had been present, the relative maximum bow C would have continued to occur at $\theta \approx 105^\circ$ and $\sin(\theta_i) \approx 0.84$, and the relative minimum bow D would have continued to occur at $\theta \approx 28^\circ$ and $\sin(\theta_i) \approx 0.94$. The presence of the first refractive index decrease does not change bows C and D since the rays responsible for these bows do not penetrate to the region of the first refractive index decrease. But since the rays responsible for bows A and B must cross the region of the second refractive index decrease on their way to and from the region of the first refractive index decrease, the second decrease influences the scattering angle of bows A and B.

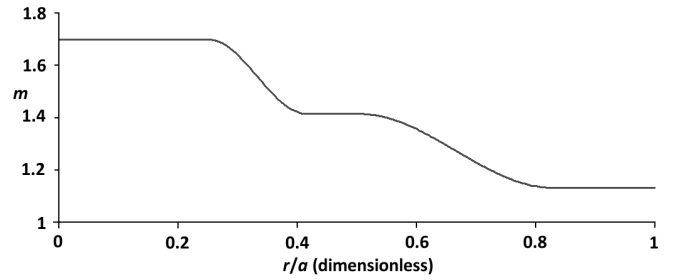


Fig. 10 Refractive index profile given by Eq. (26) using parameters $D_1 = 0.333$, $R_1 = 0.083$, $D_2 = 0.667$, $R_2 = 0.167$, $M = 1.416$ and $H_1 = H_2 = 0.142$.

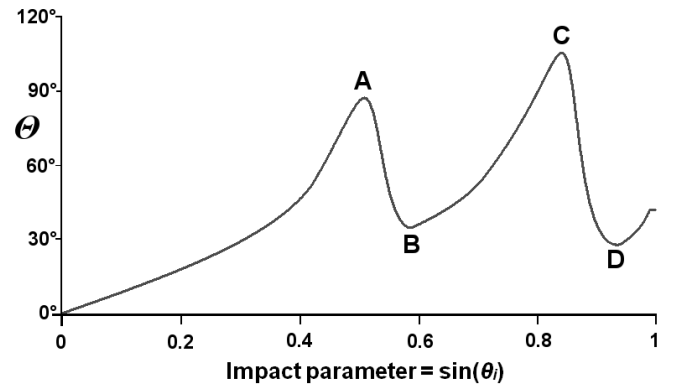


Fig. 11. Ray theory deflection angle θ as a function of $\sin(\theta_i)$ for the refractive index profile shown in Fig.10.

In order to verify the four bow prediction of ray theory, Lorenz-Mie scattering was computed for the refractive index profile of Eq. (26) with $\lambda = 0.65 \mu\text{m}$ and $a = 100 \mu\text{m}$, and is shown in Fig. 12. As before, the graph includes the contribution from all the Debye series terms. A transmission bow occurs at $\theta \approx 30^\circ$ which is the relative minimum bow D, and a wide bow-like structure is evident for $97^\circ \leq \theta \leq 107^\circ$, which is the relative maximum bow C. The two bows A and B with intermediate deflection angles are hidden in the complicated supernumerary interference pattern between bows D and C. In order to resolve these additional bows, time-domain scattering of a Gaussian pulse of full-width 5 fs and centered on $\lambda = 0.65 \mu\text{m}$ by an $a = 30 \mu\text{m}$ radially inhomogeneous sphere was computed. The results are shown in Fig.

13. All four of the transmission bows are now resolved, in agreement with the prediction of ray theory. In addition, bows A and C are easily recognized as relative maximum bows, and B and D are easily recognized as relative minimum bows.

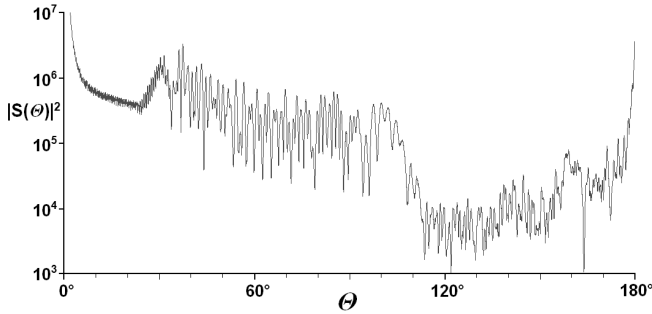


Fig. 12. Wave theory TE scattered intensity as a function of θ for an incident wavelength $\lambda = 0.65 \mu\text{m}$, a sphere of radius $a = 100 \mu\text{m}$, and the refractive index profile used in Fig. 11. The intensity has been “sun-smoothed” by convolving it with a 0.5° diameter source to remove the high-frequency interference structure.

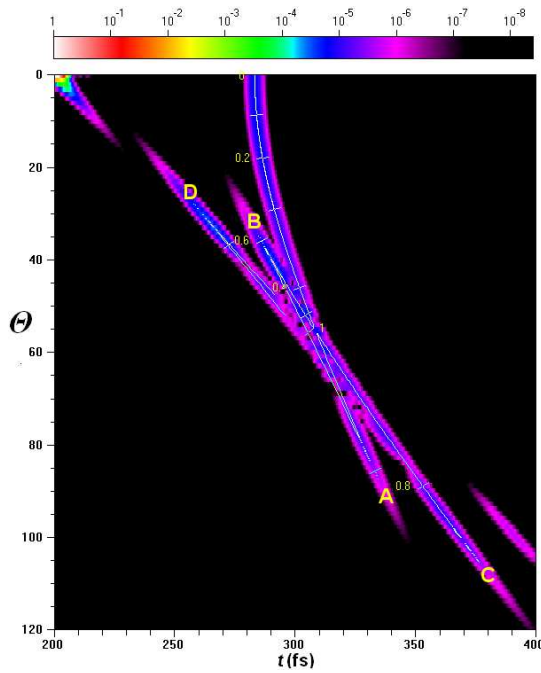


Fig. 13. (Color online) Time-domain TE scattering as a function of θ and the delay time t for a sphere of radius $a = 30 \mu\text{m}$, an incident Gaussian pulse of 5 fs full-width centered on $\lambda = 0.65 \mu\text{m}$, and the refractive index profile used in Fig. 11.

We also investigated the overarching caustic structure of the transmission bows associated with the refractive index profile of Eq. (26). The fact that zero, two, or four bows are possible by varying H_1/R_1 and H_2/R_2 initially suggested considering (i) the structurally stable elliptic and hyperbolic umbilic and swallowtail caustics [26-30], which have three control variables and partition regions containing zero, two, or four contributing rays, and (ii) the structurally stable butterfly caustic [27] which has four control variables and partitions regions containing one, three, and five contributing rays. Each of these caustics is associated with an integral over a phase function, called the generating function. The spherical symmetry of a radially inhomogeneous refractive index profile dictates that the Lorenz-Mie

scattered fields are a sum (approximated by an integral) over a single discrete variable, i.e. the partial wave number (approximated by a continuous ray impact parameter). Thus we ruled out the elliptic and hyperbolic umbilics because their phase functions are integrated over two independent variables [26,27], as occurs for scattering of a plane wave with side-on incidence by an oblate spheroid [32, 33]. We also ruled out the swallowtail caustic since it describes the transition from three bows to one bow. Although the phase function of the butterfly caustic is also integrated over only one independent variable and is cut by the θ axis zero, two, or four times, we were unable to fit the number of bows resulting from independent variation of the two steepness parameters to the geometric structure of the butterfly caustic. Rather, the independent variations of the two steepness parameters suggested a caustic structure that consisted of the direct product of two cusp caustics, each extended from two to three dimensions, and intersecting each other at an angle of 90° . The two fold lines of each cusp are extended into curved planes that have been called fold surfaces [27, 29], and the cusp point that joins the pair of folds is extended into a line that has been called a rib. For the two intersecting three dimensional cusps considered here, the two orthogonal rib lines coincide with the H_1/R_1 and H_2/R_2 axes, and the θ axis is perpendicular to them both. One way of intersecting the two cusps is the double-cusp unfolding of the 0X_9 caustic where the bisector of each of the intersecting cusps is in the θ direction (see Fig. 5 of [29] and Fig. 1b of [34]). But this geometry did not allow for the possibility of the θ axis crossing the caustic zero times, and was thus ruled out. Another way of intersecting the cusps, as shown in Fig. 14, is if the one having its rib line along the H_1/R_1 axis is oriented so that its bisector is in the H_2/R_2 direction, and the one with its rib line along the H_2/R_2 axis is oriented so that its bisector is in the H_1/R_1 direction. This structure easily conformed to the progression of the number of bows that result as H_1/R_1 and H_2/R_2 are independently varied through their full ranges. Although this caustic fitting does not constitute a proof, we provisionally suggest that this is the overarching caustic structure of the bows associated with the refractive index profile of Eq. (26).

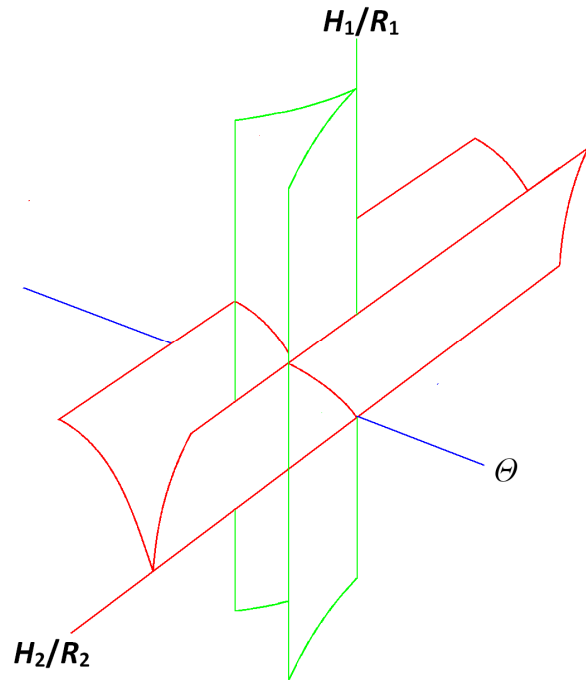


Fig. 14 (Color online) Direct product of two three-dimensional cusp caustics.

7. CONCLUSIONS

As was mentioned in Sec. 1, while no transmission bows are possible for short wavelength scattering of a plane wave by a homogeneous sphere, a number of previous authors have predicted the occurrence of various numbers of transmission bows for short wavelength scattering of a plane wave by a radially inhomogeneous sphere. But in those previous studies, no physical mechanism was given for the cause of the bows, and no specific predictions were made for the conditions on the refractive index profile under which transmission bows can be expected to occur. This study addresses these unanswered questions.

The radially inhomogeneous refractive profile $m(w)$ with $w \equiv r/a$ may be that of a particle with $m(w) \geq 1$, or a bubble with $m(w) \leq 1$. It may increase as a function of w with $dm/dw > 0$, or it may decrease with $dm/dw < 0$. It may be an edgeless particle or bubble with $m(1) = 1$, or a hard-edge particle or bubble with $m(1) \neq 1$. The function $\eta(w) = w m(w)$ may be monotonically increasing over a particular range of η , or it may not. In light of the investigations reported here, we feel that it is not possible to provide a single universal rule giving the number of transmission bows that will occur for any given refractive index profile. Rather, we believe the problem must be broken into a number of refractive index equivalence classes that are then each examined individually.

In this study we have focused on the class $m(w) > 1$, $dm/dw < 0$, and $\eta(w)$ being monotonically increasing for $0 \leq \eta \leq 1$. For this class of refractive index profiles, transmission bows occur only in pairs, a relative maximum bow followed by a relative minimum bow. Depending on the number of isolated regions of refractive index decrease and on the steepness of the decrease in each region, no pairs, one pair, two pairs, etc., can occur. Relative maximum bows were found to occur for rays that just start to penetrate to the steepest part of the region of refractive index decrease, and correspond to the near-onset of the classical phenomenon of orbiting. Relative minimum bows were found to occur for rays that just start to penetrate into the region of refractive index decrease. They correspond to increased refraction in that region when compared to the lesser refraction that would have been experienced by rays had the refractive index increase not occurred.

Similar results, mentioned at the end of Sec. 2, were obtained for a number of other refractive index equivalence classes. Using the method of analysis described here, predictions of the number of bows may also be made for families of rays that undergo one or more internal reflections before exiting the sphere. The transmission bows for short wavelength scattering predicted in the context of ray theory also are predicted to occur in wave scattering, both in the frequency-domain and in the time-domain.

Acknowledgment

The authors wish to thank Prof. John A. Adam of Old Dominion University for bringing Ref. [5] to our attention, and for several fruitful conversations during the course of this work.

APPENDIX A. SIGNATURE OF BOWS IN TIME-DOMAIN SCATTERING

The ray theory deflection angle for transmission scattering is given in Eq. (1). Let $L(\theta)$ be the optical path length of the ray trajectory divided by the sphere radius, measured from the entrance plane of the sphere to its exit plane. Also let (r, ξ) be the polar coordinates of a point on the ray trajectory with respect to the center of the sphere, and let ds be the differential arc length along the trajectory divided by the sphere radius. Then

$$L(\theta) = \int m ds = \int m(w) (ds/d\xi) (d\xi/dw) dw. \quad (\text{A1})$$

From [14] one has

$$dw/d\xi = [w / \sin(\theta)] [\eta^2(w) - \sin^2(\theta)]^{1/2}. \quad (\text{A2})$$

Substituting Eq. (A2) into Eq. (A1) along with the standard formula for the arc length in polar coordinates, adding and subtracting $\sin^2(\theta)$ to the numerator factor of the resulting expression, and then substituting Eq. (1) into the result, one gets

$$L(\theta) = 2 - 2 \cos(\theta) + \sin(\theta) [\theta(\theta) + \pi - 2\theta] + 2 \int \frac{1}{w_T} (dw/w) [\eta^2(w) - \sin^2(\theta)]^{1/2}. \quad (\text{A3})$$

Taking into account the θ_i dependence of the lower limit of integration in Eq. (A3), and assuming that orbiting does not occur, $(d\eta/dw)_{w_T} \neq 0$, the derivative of Eq. (A3) is

$$(dL/d\theta) = \sin(\theta) (d\theta/d\theta). \quad (\text{A4})$$

For the occurrence of a transmission bow at $\theta_i = \theta^R$, both the deflection angle and the optical path length are then simultaneous extrema. Taking the derivative of Eq. (A4) one obtains

$$(d^2L/d\theta^2) = \cos(\theta) (d\theta/d\theta) + \sin(\theta) (d^2\theta/d\theta^2). \quad (\text{A5})$$

Evaluating Eq. (A5) at the rainbow condition gives

$$(d^2L/d\theta^2)^R = \sin(\theta^R) (d^2\theta/d\theta^2)^R. \quad (\text{A6})$$

Thus the simultaneous extrema are both either relative maxima or relative minima.

One can Taylor series expand both θ and L about their values θ^R and L^R at a transmission bow, obtaining

$$(\theta - \theta^R) = a_2 (\theta_i - \theta^R)^2 + a_3 (\theta_i - \theta^R)^3 + O(\theta_i - \theta^R)^4, \quad (\text{A7})$$

$$(L - L^R) = b_2 (\theta_i - \theta^R)^2 + b_3 (\theta_i - \theta^R)^3 + O(\theta_i - \theta^R)^4. \quad (\text{A8})$$

Assume that θ and L are both relative minima at the bow, so that $a_2 > 0$, $b_2 > 0$, and a_3 and b_3 can be either positive or negative. If the second term on the right hand side of Eq. (A7) is much smaller than the first term, Eq. (A7) can be approximately inverted in the vicinity of the bow to give

$$(\theta - \theta^R) = \pm [(\theta - \theta^R) / a_2]^{1/2} - [a_3 / (2a_2^2)] (\theta - \theta^R) + O(\theta - \theta^R)^{3/2} \quad (\text{A9})$$

Substituting Eq. (A9) into Eq. (A8) we obtain

$$(L - L^R) = (b_2 / a_2) (\theta - \theta^R) \pm [(b_3 a_2 - b_2 a_3) / a_2^{5/2}] (\theta - \theta^R)^{3/2} + O(\theta - \theta^R)^2. \quad (\text{A10})$$

The second term on the right hand side of Eq. (A10) is a cusp about the diagonal line given by the first term. Since the delay time for time-domain scattering is

$$t = L / c \quad (\text{A11})$$

where c is the speed of light in the external medium, Eq. (A10) describes the cusp structures in the vicinity of the bows in the time-domain trajectories shown in Figs. 7 and 13. Similarly, if both θ and L are relative maxima at the transmission bow, then

$$(L - L^R) = (b_2 / a_2) (\theta - \theta^R) \mp [(b_3 a_2 - b_2 a_3) / a_2^{5/2}] (\theta - \theta^R)^{3/2} + O(\theta - \theta^R)^2, \quad (\text{A12})$$

which is again a cusp about the diagonal line given by the first term of Eq. (A12). Finally, it should be noted that a_2 , b_2 , a_3 , and b_3 are proportional to the second and third derivatives of θ and L evaluated at the bow. Making these substitutions, defining

$$h \equiv (d^2\theta/d\theta^2)^R / [2 \cos^2(\theta^R)], \quad (\text{A13})$$

and substituting the results into Eq. (A10), the phase of the rays in the vicinity of the bow from the sphere's entrance plane to its exit plane is

$$\Phi(\theta) = ka L(\theta) = ka [L^R + \sin(\theta^R) (\theta - \theta^R) \pm (2/3) h^{-1/2} (\theta - \theta^R)^{3/2} + O(\theta - \theta^R)^2]. \quad (\text{A14})$$

This has the same functional dependence as the phase of the two supernumerary rays in the two-ray limit of Airy theory that flank the $(p-1)$ -order rainbow of a homogeneous sphere (see Eqs.(4, 24, 25) of [9], Eqs.(6.24, 6.31) of [10], and Eqs.(10, 16) of [35]). The Airy theory scattered electric field for a radially inhomogeneous sphere has been derived as an approximation to the exact wave theory solution to the electromagnetic boundary value problem and will be published separately. The value of h obtained in that analysis agrees with Eq.

(A13), and the conjectured overall caustic morphology of Figs. 6, 8 and illustrated in Fig. 9 is derived.

REFERENCES

1. C. F. Bohren and A. B. Fraser, "Newton's zero-order rainbow: Unobservable or nonexistent?" *Am. J. Phys.* **59**, 325-326 (1991).
2. A. E. Shapiro, "Comment on 'Newton's zero-order rainbow: Unobservable or nonexistent?'" *Am. J. Phys.* **60**, 749-750 (1992).
3. J. A. Lock and T. A. McCollum, "Further thoughts on Newton's zero-order rainbow," *Am. J. Phys.* **62**, 1082-1089 (1994).
4. J. A. Lock, "Ray scattering by an arbitrarily oriented spheroid. II. Transmission and cross-polarization effects," *Appl. Opt.* **35**, 515-531 (1996).
5. W. S. Jagger, "The optics of the spherical fish lens," *Vision Res.* **7**, 1271-1284 (1992).
6. J. A. Adam and P. Laven, "Rainbows from inhomogeneous transparent spheres: A ray-theoretic approach," *Appl. Opt.* **46**, 922-929 (2007).
7. J. A. Adam, "Zero-order bows in radially inhomogeneous spheres: Direct and inverse problems," *Appl. Opt.* **50**, F50-F59 (2011).
8. J. A. Lock, P. Laven, and J. A. Adam, "Scattering of a plane electromagnetic wave by a generalized Luneburg sphere-Part 1: Ray theory," *J. Quant. Spectrosc. Radiat. Transfer* **162**, 154-163 (2015).
9. K. W. Ford and J. A. Wheeler, "Semiclassical description of scattering," *Ann. Phys. (N.Y.)* **7**, 259-286 (1959).
10. M. V. Berry and K. E. Mount, "Semiclassical approximations in wave mechanics," *Rep. Prog. Phys.* **35**, 315-397 (1972).
11. H. Goldstein, *Classical Mechanics, second ed.*, (Addison-Wesley, Reading MA, 1980), pp. 111-112.
12. N. F. Mott and H. S. W. Massey, *The theory of atomic collisions*, (Clarendon Press, Oxford U.K., 1987), pp. 106-110.
13. R. G. Newton, *Scattering Theory of Waves and Particles*, (McGraw-Hill, New York, 1966), pp. 581-582.
14. M. Born and E. Wolf, *Principles of Optics, sixth ed.*, (Cambridge U. Press, Cambridge U.K., 1998) pp. 123-124.
15. H. M. Nussenzveig, *Diffraction Effects in Semiclassical Scattering*, (Cambridge U. Press, Cambridge U.K., 1992), p.2.
16. J. O. Hirschfelder, C.F. Curtis, and R.B. Bird, *Molecular Theory of Gases and Liquids*, (Wiley, New York, 1954), pp. 552-557.
17. K. W. Ford and J. A. Wheeler, "Application of semiclassical scattering analysis," *Ann. Phys. (N.Y.)* **7**, 287-322 (1959).
18. J. A. Lock, "Scattering of an electromagnetic plane wave by a Luneburg lens. II. Wave theory," *J. Opt. Soc. Am. A* **25**, 2980-2990 (2008).
19. J. A. Lock, P. Laven, and J.A. Adam, "Scattering of a plane electromagnetic wave by a generalized Luneburg sphere-Part 2: Wave scattering and time-domain scattering," *J. Quant. Spectrosc. Radiat. Transfer* **162**, 164-174 (2015).
20. J. A. Lock, "Scattering of an electromagnetic plane wave by a Luneburg lens. I. Ray theory," *J. Opt. Soc. Am. A* **25**, 2971-2979 (2008).
21. P. Pechukas, "Time-dependent semiclassical scattering theory. I. Potential scattering," *Phys. Rev.* **181**, 166-174 (1969).
22. J. A. Lock, "Debye series analysis of scattering of a plane wave by a spherical Bragg grating," *Appl. Opt.* **44**, 5594-5603 (2005).
23. J. A. Lock, "Scattering of an electromagnetic plane wave by a Luneburg lens. III. Finely stratified sphere model," *J. Opt. Soc. Am. A* **25**, 2991-3000 (2008).
24. P. Laven, "Separating diffraction from scattering: The million-dollar challenge," *Journ. Nanophotonics* **4**, 041593 (2010).
25. P. Laven, "Time domain analysis of scattering by a water droplet," *Appl. Opt.* **50**, F29-F38 (2011).
26. M. V. Berry, "Waves and Thom's theorem," *Adv. Phys.* **25**, 1-26 (1976).
27. M. V. Berry and C. Upstill, "Catastrophe optics: Morphologies of caustics and their diffraction patterns," *Prog. Opt.* **18**, 257-346 (1980).
28. J. Walker, "Caustics: mathematical curves generated by light shined through rippled plastic," *Sci. Am.* **249**, 190-202 (1983).
29. F. Wright, "Catastrophe optics," *Phys. Bulletin* **39**, 313-316 (1988).
30. P. L. Marston, "Geometrical and catastrophe optics methods in scattering," *Phys. Acous.* **21**, 1-234 (1992).
31. J. A. Lock and C. L. Adler, "Debye-series analysis of the first-order rainbow produced in scattering of a diagonally incident plane wave by a circular cylinder," *J. Opt. Soc. Am. A* **14**, 1316-1328 (1997).
32. P. L. Marston and E. H. Trinh, "Hyperbolic umbilic diffraction catastrophe and rainbow scattering from spheroidal drops," *Nature* **312**, 529-531 (1984).
33. J. F. Nye, "Rainbow scattering from spheroidal drops – an explanation of the hyperbolic umbilic foci," *Nature* **312**, 531-532 (1984).
34. C. Upstill, F. J. Wright, J. V. Hajnal, and R. H. Templer, "The double-cusp unfolding of the O_9 diffraction catastrophe," *Opta Acta* **29**, 1651-1676 (1982).
35. M. V. Berry, "Uniform approximation for potential scattering involving a rainbow," *Proc. Phys. Soc.* **89**, 479-490 (1966).